The Astronomical Journal, 126:1286–1294, 2003 September

Hα + [N II] OBSERVATIONS OF THE H II REGIONS IN M81

Weipeng Lin,[1,2,3] Xu Zhou,[2,3] David Burstein,[4] Rogier A. Windhorst,[4] Jiansheng Chen,[2,3] Wen-ping Chen,[5] Zhaoji Jiang,[2] Xu Kong,[6] Jun Ma,[2] Wei-hsin Sun,[5] Hong Wu,[2] Suijian Xue,[2] and Jin Zhu[2]

Received 2002 March 7; accepted 2003 June 13

ABSTRACT

In a first of a series of studies of the Hα + [N II] emission from nearby spiral galaxies, we present measurements of Hα + [N II] emission from H II regions in M81. Our method uses large-field CCD images and long-slit spectra and is part of the ongoing Beijing-Arizona-Taipei-Connecticut Sky Survey (the BATC survey). The CCD images are taken with the National Astronomical Observatories of China (NAOC) 0.6/0.9 m f/3 Schmidt telescope at the Xinglong Observing Station, using a multicolor filter set. Spectra of 10 of the brightest H II regions are obtained using the NAOC 2.16 m telescope with a Tek 1024 × 1024 CCD. The continua of the spectra are calibrated by flux-calibrated images taken from the Schmidt observations. We determine the continuum component of our Hα + [N II] image via interpolation from the more accurately measured backgrounds (M81 starlight) obtained from the two neighboring (in wavelength) BATC filter images. We use the calibrated fluxes of Hα + [N II] emission from the spectra to normalize this interpolated, continuum-subtracted Hα + [N II] image. We estimate the zero-point uncertainty of the measured Hα + [N II] emission flux to be ∼8%. A catalog of Hα + [N II] fluxes for 456 H II regions is provided, with those fluxes being on a more consistent linear scale than previously available. The logarithmically binned Hα + [N II] luminosity function of H II regions is found to have slope $\alpha = -0.70$, consistent with previous results (which allowed $\alpha = -0.5$ to -0.8). From the overall Hα + [N II] luminosity of the H II regions, the star formation rate of M81 is found to be $\sim 0.68\ M_{\odot}\ \mathrm{yr}^{-1}$, modulo uncertainty with extinction corrections.

Key words: galaxies: individual (M81) — galaxies: photometry — H II regions

On-line material: machine-readable table

1. INTRODUCTION

Part of the Beijing-Arizona-Taipei-Connecticut (BATC) Sky Survey is to do emission-line studies of Hα + [N II] emission from large appearing, nearby spiral galaxies that are well suited to our imaging setup. M81 is a well-known, nearby Sab galaxy (3.6 Mpc; cf. Freedman et al. 1994) that exhibits both LINER and Seyfert 1 characteristics. It is useful as the first galaxy to study in our program, since many studies have been made of the structure and star-forming regions of M81, as well as of its nucleus (e.g., Keel 1989; Hill et al. 1992; Adler & Westpfahl 1996; Davidge & Courteau 1999; Grossan et al. 2001). The H II regions of M81 have been studied by Hodge & Kennicutt (1983a, 1983b), Stauffer & Bothun (1984), Kaufman, Kennicutt, & Bash (1986), Kaufman et al. (1987), Garnett & Shields (1987), Petit, Sivan, & Karachentsev (1988), and Devereux, Jacoby, & Ciardullo (1995). However, the existing optical photometry of the H II regions is photographic (Kaufman et al. 1986; Petit et al. 1988, hereafter PSK88), which is not sufficiently accurate for Hα + [N II] flux determinations.

Devereux et al. (1995) previously obtained an Hα + [N II] image of M81 using CCD data, in which they point out that a small uncertainty (3%) in the continuum level translates into a large (∼30%) uncertainty in the measured Hα + [N II] flux. Greenawalt et al. (1998) studied the diffuse ionized gas (DIG) in M81 and attributed about half of the Hα (i.e., no [N II]) emission to the DIG. In the current paper, we combine accurate photometric observations of M81 with new spectroscopic observations of the H II regions to obtain new, independent, measurements of the Hα + [N II] flux emitted from M81 H II regions. Section 2 describes the observations and data reduction procedures used for both the images and the spectra, which employ a new method to reduce the uncertainty in the continuum background of our image. This new method results in more accurate measurements of the Hα + [N II] flux from the M81 H II regions. We discuss our errors of measurement and some statistical applications our data can provide in § 3. We summarize our results in § 4.

2. OBSERVATIONS AND DATA REDUCTION

2.1. *Spectroscopic Observations*

Spectra of the nucleus of M81 and its H II regions were obtained using the 2.16 m telescope at Xinglong Station of the National Astronomical Observatories of China (NAOC) between 1997 April 9 and 11. A Zeiss universal spectrograph using a Tek 1024 × 1024 CCD and a grating of 200 Å mm^{-1} dispersion was used to obtain a spectral resolution of 10.0 Å over the range 4500–9500 Å, centered near 7000 Å. It was necessary to restrict our spectroscopic observations to the brightest H II regions, owing to the bright background of M81 (see Fig. 1). In most cases, a slit width

[1] The Partner Group of MPI für Astrophysik, Shanghai Astronomical Observatory, Shanghai 200030, China; linwp@center.shao.ac.cn.

[2] National Astronomical Observatories, Chinese Academy of Sciences, Beijing 100012, China.

[3] Beijing Astrophysics Center and Department of Astronomy, Peking University, Beijing 100871, China.

[4] Department of Physics and Astronomy, Box 871504, Arizona State University, Tempe, AZ 85287-1504.

[5] Institute of Astronomy, National Central University, Chung-Li 32054, Taiwan.

[6] Center for Astrophysics, University of Science and Technology of China, Hefei 230026, China.

TABLE 1
SPECTRAL OBSERVATIONS OF THE M81 H II REGIONS

Name of Spectrum	PSK No.[a]	R.A. (J2000.0)	Decl. (J2000.0)	Slit Width (arcsec)	No. of Exposures (s)
M81-266	266	09 55 41.1	68 59 44.7	3	3 × 1200
M81-311	311	09 55 53.2	68 59 04.2	3	3 × 1200
M81-178	178	09 55 16.7	69 08 56.6	3	3 × 1200
M81-209	209	09 55 25.0	69 08 16.4	3	3 × 1200
M81-15	15	09 54 39.3	69 05 26.9	3	3 × 1200
M81-16	16, 12, 19	09 54 39.6	69 04 47.8	3	3 × 1200
M81-17	17	09 54 39.8	69 05 02.2	3	3 × 1200
M81-23	23, 25	09 54 41.4	69 04 07.5	3	3 × 1200
M81-29	29, 30, 31	09 54 42.6	69 03 36.9	3	3 × 1200

NOTE.—Units of right ascension are hours, minutes, and seconds, and units of declination are degrees, arcminutes, and arcseconds.
[a] PSK No. refers to the H II region index in the catalog of Petit et al. (1988).

of 3″ was chosen to match the seeing disk at Xinglong (typically ~2″). Often the 4′ long slit was rotated to include more than one H II region at one time. Since our slit was never free of galaxy light, separate sky exposures were periodically taken.

The data were reduced using the MIDAS package. The response of the instrument was calibrated by standard stars HZ 44, HD 74721, Feige 98, and Feige 56. The details of the observation and data reduction are described by Kong et al. (1999, 2000). Table 1 gives the 10 H II regions observed spectroscopically. Table 3 gives the results for measurement of Hα + [N II] emission from these 10 H II regions derived from these spectra, together with estimated errors.

2.2. *Image Observations*

The images used in this paper were taken with 0.6/0.9 m f/3 Schmidt Telescope of at the Xinglong Observing Station of NAOC, equipped with a Ford 2048 × 2048 CCD camera mounted at its focus. The field of view of the CCD is close to 58′ × 58′, with a scale of 1.″7 pixel^{-1}. The four filters used for this study are a subset of the 15 intermediate-band filters used for the BATC Multicolor Sky Survey (cf. Fan et al. 1996; Yan et al. 2000). This filter system was designed to minimize the effect of night-sky emission lines, especially those in the near-infrared that are both bright and highly variable. The observations reported here were taken on 30 individual nights over the time period 1995 February 5 to 1997 February 19. Images in each filter were dithered to provide accurate cosmic-ray and defect subtraction. Both M81 and M82 comfortably fit within this field of view.

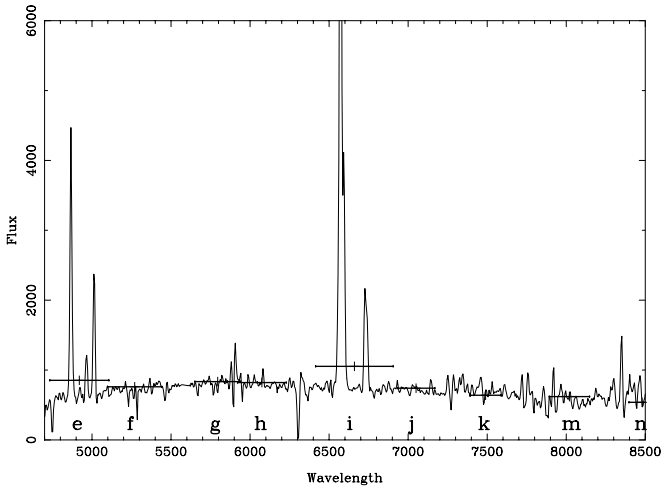

FIG. 1.—Example of spectrum for the M81 H II No. 16 region listed in Tables 1 and 3. Note that the fluxes in BATC passbands are also shown as thick horizontal lines from left to right for BATC filters *e*, *f*, *g*, *h*, *i*, *j*, *k*, and *m* (cf. Zhou et al. 2001, 2003), as well as the narrow Hα filter *t*. Calibration of the continuum spectrum was made using the calibrated observations of M81 made in these BATC filters.

The Hα images were taken by using our "*t* filter" (see Table 2), which has a central wavelength of 6600 Å and a full width at half-maximum (FWHM) of 120 Å. The transmission profile of our *t* filter is presented in Figure 2. As is evident, the *t*-filter flux includes emission by [N II] line at 6584 Å, as well as emission from Hα, which is common in such investigations (cf. Devereux et al. 1995). Three of the nominal BATC filters cover this spectral range: the *h* filter and *j* filter on either side of Hα (central wavelengths of 6075 and 7050 Å and FWHM of 310 and 300 Å, respectively) and the *i* filter, which is a wider filter (FWHM = 480 Å), also centered near Hα (central wavelength of 6660 Å) (the transmission profiles for these filters can be found in Zhou et al. 2003). A total of 51 images were obtained in the four filters with a total exposure time of close to 14 hr. The field observed is centered at R.A. = $09^{h}55^{m}35\overset{s}{.}25$ and decl. = 69°21′50.″9 (J2000.0).

Details of the flat fielding and flux calibration of the BATC CCD system that we employ at the Xinglong Schmidt telescope have been described in detail elsewhere (cf. Fan et al. 1996; Zheng et al. 1999; Yan et al. 2000; Zhou et al. 2001; Wu et al. 2002; Zhou et al. 2003). The reader is referred to those papers for a detailed description. Calibration of the BATC observations in terms of flux using Oke & Gunn (1983) standard stars is also detailed in Yan et al. (2000). Briefly, our system employs a diffuser plate placed in front of the Schmidt corrector plate to provide a sky-consistent, high signal-to-noise ratio (S/N) flat field for this CCD system, since the sky itself is not flat over the 1° size scale of our CCD. On nights that are photometric, we observe the Oke & Gunn (1983) primary flux standard stars HD 19445, HD 84937, BD +26°2606, and BD +17°4708 (cf. Yan et al. 2000), which provide us direct calibration of our filter observations in terms of flux.

TABLE 2
IMAGE OBSERVATIONS IN Hα AND NEARBY BANDS

Filter	Wavelength (Å)	FWHM (Å)	Exposure (s)	No. of Images	No. of Calibration Images
t	6600	120	23700	16	...
h.....	6075	310	8040	10	3
i.....	6660	480	9960	14	5
j.....	7050	300	8340	11	4

2.3. *Image Data Reduction*

The initial reduction of the images is done by the PIPELINE 1 system software that was developed for automatic data reduction of images taken for the BATC multicolor sky survey (cf. Fan et al. 1996 for details). In the PIPELINE 1 system, images are bias-subtracted, dark-count–subtracted, and flat-fielded using multiple biases, dark frames, and dome flats taken through the diffusing plate in front of the Schmidt telescope corrector lens. The high accuracy of this procedure has been demonstrated in our previous papers (Fan et al. 1996; Zheng et al. 1999; Yan et al. 2000; Wu et al. 2002). The dithered, flat-fielded images in each passband are combined by integer pixel shifts. Cosmic rays and bad pixels are removed by comparison among the images during combination. Images are then recentered, and the position of the center and all objects on the image are accurately tied to the J2000.0 coordinate system via the STScI Guide Star Catalog (Lasker et al. 1990). These images are flux-calibrated using the Oke-Gunn standard-star observations, as detailed in our previous papers (Fan et al. 1996; Yan et al. 2000; Zhou et al. 2001, 2003).

We employ the method of Zheng et al. (1999) and Wu et al. (2002; please see those papers for details of our methodology) to accurately determine the sky background in all three filters. Briefly, areas around M81 and M82 are first masked; M81 via a circle of 400 pixels in radius (22.′7 in diameter) and M82 via a circle of 200 pixels in radius (11.′4 in diameter). Stars are removed at less than 5% of the sky level (cf. Zheng et al. 1999 and Wu et al. 2002) via point-spread function (PSF) fitting and subtraction. The remaining areas around stars are then masked. The sky background is fitted, using only the unmasked areas and the same method as employed by Zheng et al. A smoothed version of the masked image is produced by mode-filtering the image with a box 10×10 pixels in size. We then fitted to each row of the smoothed and masked image a one-dimensional Legendre function on the order of three or less, rejecting points above 2 σ on the high side and 3 σ on the low side. The reason for the asymmetric rejection of points is that the main sources of scatter on the high side are faint, undetected sources and unfitted faint wings of stars, while the low side values result from statistical fluctuations.

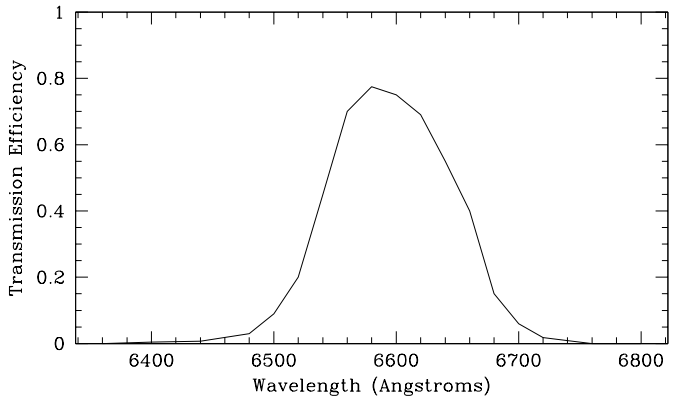

FIG. 2.—Transmission profile of the Hα-redshifted *t* filter

The sky background that is fitted is then subtracted from the *h*, *j*, and *t* images. The continuum component (stellar flux from M81) of the summed *t* filter is obtained not from the image itself, but rather via interpolation of the stellar flux interpolated from the summed *h* and *j* images, suitably normalized by exposure times as follows:

$$\mathrm{Cont}_t = 0.45\mathrm{Cont}_h + 0.55\mathrm{Cont}_j \ . \qquad (1)$$

We then select ~50 unsaturated stars over the whole field of view and adjust the interpolated values from the summed *h* and *j* images such that these stars disappear. By doing this, we also properly scale the M81 stellar background in this interpolated image, assuming that none of these stars have emission lines in their spectra (and none did). The result of this sky background, stellar M81 subtracted Hα + [N II] image is shown in Figure 3. It is evident from Figure 3 that all M81 starlight, as well as the flux from all foreground stars (not just the ones that are zeroed by our normalization process), are cleanly subtracted in the *t* image via this interpolation procedure (modulo saturated stars).

To further demonstrate how well our subtraction procedure worked, Figure 4 shows 1 pixel wide, 600 pixel long slices through the *t* image shown in Figure 3. Figures 4*a*–4*d* are the slices through galaxy center. As can be seen, these slices go through several H II regions. (The center region is not shown in these slices, since steep luminosity gradients in the center of M81, combined with our lower angular resolution and slight mismatches in registration of images, result in large fluctuations in brightness on this scale from the continuum subtraction process.) It is evident from all six slices in Figure 4 that our continuum subtraction process has worked well in removing background flux in the Hα part of the spectrum in our image (cf. the magnified view given in slices [*c*] and [*f*] of Fig. 4). Quantitatively the rms statistical error in the background in the continuum-subtracted image is close to 15 ADU pixel^{-1} (close to 1.8×10^{-16} ergs s^{-1} cm^{-2} pixel^{-1}), with an overall zero-point residual of only 2 ADU pixel^{-1} (2.4×10^{-17} ergs s^{-1} cm^{-2} pixel^{-1}). The random background error of 15 ADU pixel^{-1} can be reduced by $1/\sqrt{n}$, where *n* is the number of the pixels sampled.

The small zero-point error introduced resulting from our subtraction process does not enter significantly into the

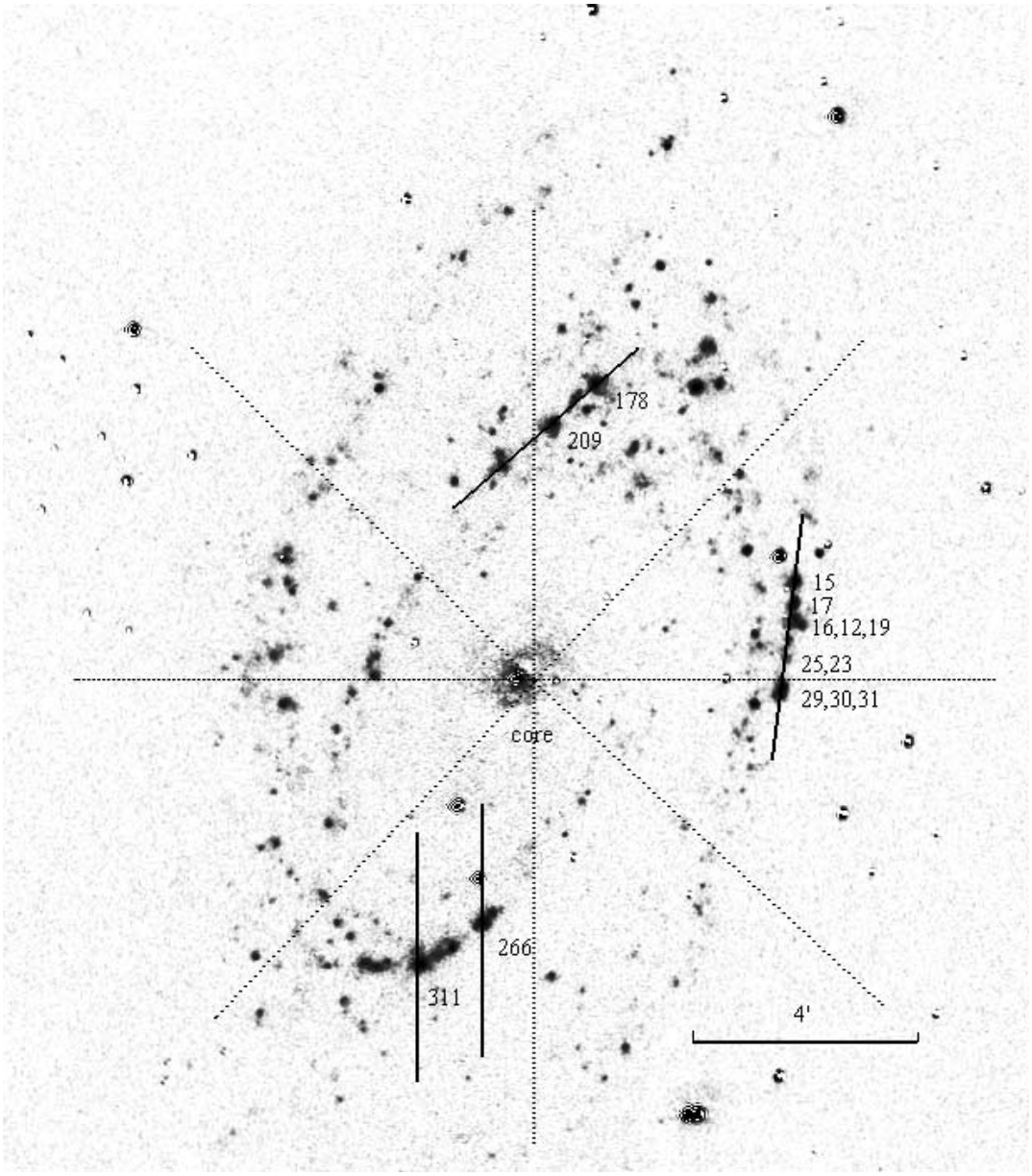

FIG. 3.—Sky background–subtracted Hα image. The positions of long-slit spectroscopic observations are overlaid as solid lines. Slices taken through this image to test for accuracy of background subtraction are given as dotted lines. The PSK88 numbers of the H II regions are also given. Note that up is north and left is east.

errors for the fluxes of the H II regions. This is because in the vicinity of every H II region there is always some diffuse emission that makes the boundaries of H II regions vague. Hence, we are specific about the area used around each H II region that was sampled to produce its reported flux. The error and S/N for the Hα + [N II] fluxes from the H II regions in this paper include just the calibration error and the random background error for each region; zero-point errors in the continuum-subtracted image are thus included in the background subtraction for each H II region. As stated above, we only use those H II regions with S/N values for their fluxes that are 3 σ or higher.

2.4. *Flux Measurements and Calibration of the* Hα *Emission*

The Hα + [N II] emission from the M81 H II regions are calibrated by the Hα + [N II] emission we measure for the 10 H II regions with reasonably high S/N spectra in the 2.1 m data. To do so, we employ the intermediate-band fluxes in our images that we obtain for M81 outside the H II regions via our standard-star calibrations. In Table 3, we give the combined Hα + [N II] emission flux in the continuum flux-calibrated spectra together with the ADU counts for Hα + [N II] emission as measured from our image.

Figure 5 shows the relationship we derive between the Hα + [N II] fluxes from the H II regions obtained from the spectra and the ADU counts we measure for these same H II regions from the continuum-subtracted *t* image. It is evident that there is a good relationship between spectra-derived fluxes and ADU values on the image, yielding a relation of

$$\mathrm{Flux}(\mathrm{H}\alpha + [\mathrm{N\,II}]) = (1.34 \pm 0.10) \times 10^{-4}\ \mathrm{ADU}(\mathrm{H}\alpha + [\mathrm{N\,II}])\ , \quad (2)$$

TABLE 4
CATALOG OF OPTICAL BRIGHT H II REGIONS WITH Hα FLUX

No. (1)	α (2)	δ (3)	X (4)	Y (5)	Flux (6)	Err. (7)	D (8)	Flux* (9)	S/N (10)
1.....	09 54 19.82	69 07 53.1	−392.1	238.1	47	7	6.6	55	6.9
2.....	09 54 23.99	69 08 02.2	−369.8	247.2	132	8	6.6	52	17.3
3.....	09 54 33.49	69 09 04.8	−318.8	309.8	1	5	5.5	28	0.3
4.....	09 54 34.67	69 05 52.2	−313.2	117.2	477	10	6.6	866	45.8
5.....	09 54 36.10	69 06 30.5	−305.4	155.5	599	14	12.0	213	42.9
6.....	09 54 35.74	69 09 04.3	−306.8	309.3	241	10	8.8	83	23.3
7.....	09 54 36.08	69 07 16.2	−305.4	201.2	391	12	9.7	138	32.9
8.....	09 54 36.60	69 06 32.3	−302.7	157.3	482	11	9.7	242	43.9
9.....	09 54 36.27	69 07 15.4	−304.3	200.4	538	14	12.0	230	37.3
10.....	09 54 37.17	69 04 57.8	−300.1	62.8	129	44	6.6	42	3.0
11.....	09 54 37.35	69 06 35.5	−298.7	160.5	235	9	6.6	38	26.8
12.....	09 54 38.53	69 04 42.2	−292.8	47.2	1754	56	10.5	881	31.2
13.....	09 54 38.73	69 06 49.1	−291.3	174.1	163	12	7.9	78	13.7
14.....	09 54 39.15	69 05 35.1	−289.3	100.1	480	50	7.9	79	9.6
1993J	09 55 24.72	69 01 15.0	−45.5	−160.0	582	19	13.6	...	30.6

NOTE.—Table 4 is presented in its entirety in the electronic edition of the Astronomical Journal. A portion is shown here for guidance regarding its form and content.

on average, are 2.″5 larger in radius than those of PSK88. Because of the low space resolution of our images, when we made independent flux measurements of H II regions using the "SExtractor" code (Bertin 1996), the number of regions found was less than that of PSK88. This depends on what threshold of flux and other parameters for the detection. Thus for simplicity, we adopt the positions of H II regions provided by PSK88.

2.5. *The* H II *Region Catalog*

The resulting coordinates and fluxes of the H II regions are listed in Table 4. The galaxy center of M81 is located at $\alpha = 09^{h}55^{m}33\overset{s}{.}2$, $\delta = +69^{\circ}03'55''$ (J2000.0). In this table, column (1) is the PSK88 number for the H II region; columns (2) and (3) give the right ascension and declination coordinates (J2000.0) of the H II regions; columns (4) and (5) list the X and Y distance from the galaxy center, in units of arcseconds; columns (6), (7), and (9) list the Hα + [N II] flux measured in this paper for this H II region, its 1 σ uncertainty, and the PSK88 flux (Flux*), respectively, in units of 10^{-16} ergs s^{-1} cm^{-2}; column (8) is the diameter of the circular aperture used to measure the flux for each H II region, in units of arcseconds; and column (10) is the S/N value for each H II region from our measurement. Kindly note that the direction of X (or Y) axis is the same as right ascension (or declination).

Please note that our X and Y values are slightly different than those of PSK88 because our astrometry puts the center of M81 in a different location, with an additional rotation of the field of view. Of the 492 H II regions for which we have obtained Hα + [N II] fluxes, 93% (456) have those fluxes determined to an accuracy of 3 σ or greater. We will only use these more accurately determined fluxes in our analysis.

3. ESTIMATION OF ERRORS AND DISCUSSION

Our errors come from a combination of errors in H II region pointing during the spectral observations, differences of matching the area of the H II regions on the image to that covered by the spectra, the seeing difference between the image and the spectra, flux calibration of the image observations, and how well we can continuum-subtract the background from the H II regions on the Hα image.

3.1. *Pointing Errors*

For the 10 bright H II regions for which we obtained spectra, we define on the Hα image the same rectangle area in the same direction as the spectrograph slit. Fortunately, the seeing of the spectroscopic observations is similar to that of the CCD image, 4″ ± 0.″2. Our internal estimate of the error of telescope pointing (obtained from the PIPELINE 1 fit to the Lasker et al. stars) is 0.″3. Assuming the PSF is Gaussian with a FWHM of 4″, we calculate the ratio of flux for various stars for offsets in position up to 0.5 pixels (0.″85) for the spectroscopic slit width. We find that the difference is 0.02 mag when the offset is 0.5 pixels. We therefore conclude that the uncertainty from telescope pointing introduced into our data is less than 0.02 mag.

3.2. *Absolute Calibration and Linearity*

As shown in Figure 3 and § 2.4, we match the Hα + [N II] fluxes from our spectral observations to the ADU counts on the continuum-subtracted image to an accuracy of 7%. Any error caused by mismatch of slit area with image area for these H II regions is subsumed into this calibration. As discussed in previous papers from our program (Fan et al. 1996; Yan et al. 2000; Zhou et al. 2001, 2003), the uncertainty in calibrating the intermediate-band images is generally less than 0.02 mag, or 2% in flux. To be more conservative, we allow an error of 3% in flux. Taken together in quadrature, this yields a total zero-point absolute spectrophotometry calibration error of close to 8%.

We demonstrate the overall linearity of the Hα image by differentially comparing the fluxes determined for the H II regions from the Hα + [N II] t image with those determined for those same regions from the wider, intermediate-band i image that covers this spectral region. This is shown in Figure 6, where we plot the difference, Hα + [N II] flux from the t image minus that obtained from the i-band image versus the t image Hα + [N II] flux for the brighter H II regions,

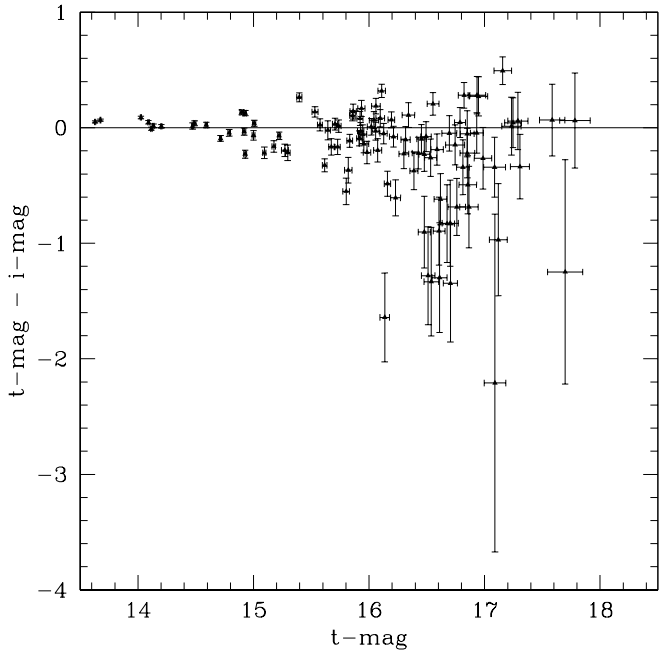

FIG. 6.—Plot of *t* magnitude (the Hα instrumental magnitudes measured from continuum-subtracted *t*-filter image) vs. the difference between *t* magnitude and *i* magnitude (the instrumental magnitudes measured from the continuum-subtracted *i*-filter image). See main text for details.

including the 10 brightest H II regions that were used for the spectral line calibration.

In this comparison, the *i*-band magnitudes are set so that the *i*-band magnitudes for bright H II regions are equal to the corresponding *t*-band magnitudes, since what is relevant in this comparison is the linearity of the Hα scale. Further, for this comparison, we do not subtract the background of M81 for the *i*-band H II regions. We also note that the BATC *i* filter also includes emission from [S II] doublet at 6717 and 6737 Å, further complicating this comparison. As such, we limit our comparison to the brighter H II regions. As can be seen in Figure 6, these two independent magnitude measures of the H II regions of M81 are reasonably linear.

3.3. *Comparison with Previous Work*

The H II region fluxes measured by PSK88 were made from photographic plates. As such, we might expect some systematic differences between their fluxes and ours as a function of position on M81, given the well-known difficulty of flat-fielding photographic images. In Figure 7*a*, we show the ratio of fluxes, this paper to that of PSK88, as a function of our fluxes. Given that our apertures are larger than those of PSK88, we naturally expect our fluxes to be higher, which is what we find. We also find there to be a systematic effect over the field of view. Figure 7*b* shows the ratio used in Fig. 7*a* plotted versus radial position from the center of the galaxy.

As is evident, there is a systematic difference in fluxes as a function of increasing distance going from the southeast to the northwest part of M81. On this same graph, we plot (with filled symbols) the difference between our Hα fluxes and our *i*-band fluxes (*t* flux/*i* flux) along the same diagonal. Since there is no evidence that such a systematic error exists in our data, we conclude that the photographic data of PSK88 contains this error.

3.4. *Total* Hα *Flux From Observed M81* H II *Regions and SN 1993J*

The total Hα + [N II] flux of all the H II regions (with S/N $\geq 3\ \sigma$) in M81 is $\sim 2.26 \times 10^{-11}$ ergs s^{-1} cm^{-2}, which corresponds to a luminosity of $\sim 8.7 \times 10^{6}\ L_{\odot}$ (the fainter, lower S/N H II regions in M81 contribute less than 1% additional flux). The total Hα + [N II] flux we measure is half of

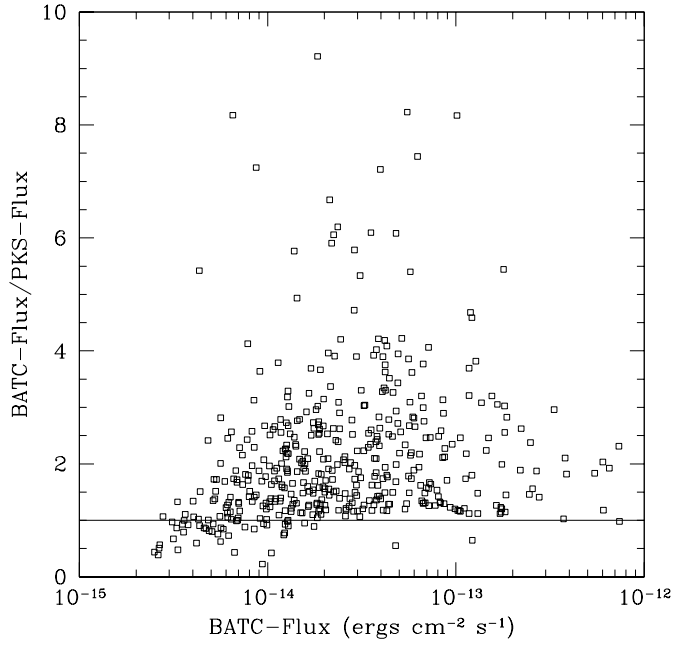

FIG. 7*a*

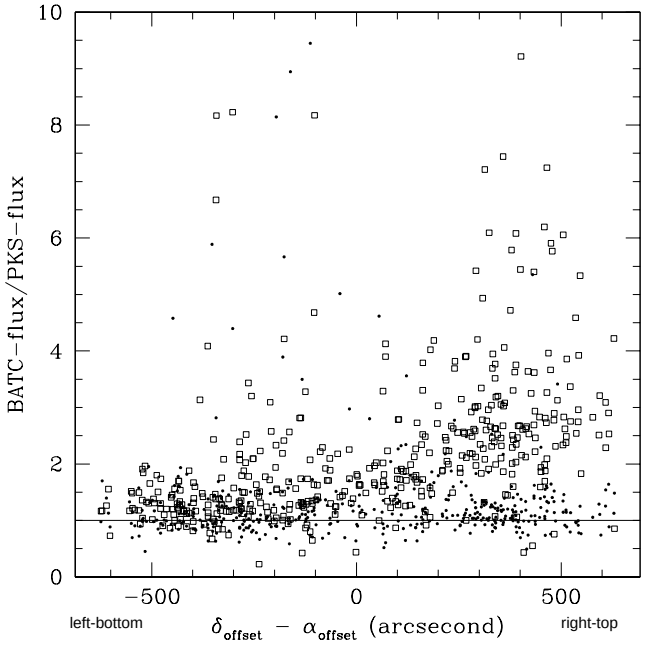

FIG. 7*b*

FIG. 7.—*Left*: Plot of the ratio of flux to PSK88 flux vs. BATC flux. *Right*: Plot of the ratio of BATC flux to PSK88 flux vs. $\delta_{\rm offset} - \alpha_{\rm offset}$ going in a diagonal from the southwest (*bottom left*) to the northeast (*top right*), as indicated by the dashed line in Fig. 3.

the overall Hα + [N II] emission coming from M81, $(1.77 \pm 0.53) \times 10^7$ $L_\odot$ (Devereux et al. 1995; including both H II region and diffuse emission-line flux). Similarly, the study of Greenawalt et al. (1998) attributes about half of the Hα emission to the DIG, so the effect of adding in the [N II]] emission to the Hα emission seems not to affect this ratio. In addition, Devereux et al. (1995) find that about 17% of the flux is due to emission by the nuclear spiral, leaving one-third of the Hα + [N II] flux from M81 coming from its diffuse interstellar medium.

We also note that we detect extra Hα + [N II] emission located at an inner arm of M81 at pixel position of (926.4, 428.6), corresponding to $\alpha = 09^h55^m24^s.7$, $\delta = +69^\circ01'15''$ (J2000.0). The position is consistent with that of the X-ray source studied by Immler & Wang (2001). Therefore, we identify this emission spot as coming from the remnant of the Type IIb supernova SN 1993J (cf. Fig. 2.). The flux is 5.8×10^{-14} ergs s^{-1} cm $^{-2}$, measured over the time period 1995 February 11–19.

3.5. *The Luminosity Function of H81* H II *Regions*

The Hα + [N II] luminosity functions of the H II regions in M81 have been determined before (cf. PSK88 and references therein; Kennicutt, Edgar, & Hodge 1989), primarily in the form of a power law. As Scoville et al. (2001) point out, angular resolution issues cause ground-based data to blend H II regions together, relative to better resolved images. This is especially true for the BATC data, which has a relative poor angular resolution (FWHM = 4″). Following Scoville et al., we define the differential form of the luminosity function as

$$\frac{dN(F_{\mathrm{H}\alpha})}{d\ln F_{\mathrm{H}\alpha}} = N_{\mathrm{up}}\left(F_{\mathrm{H}\alpha}/F_{\mathrm{up}}\right)^{\alpha}\ , \qquad (3)$$

where F_{up} is the Hα for the brightest H II region, $F_{\mathrm{H}\alpha}$ is the flux measured, and N_{up} is approximately the number of regions between $0.5F_{\mathrm{up}}$ and F_{up} for $\alpha \sim 1$. We selected only those H II regions with S/N $\geq$ 3 (456 regions in total) and apply the linear fitting using equation above. The slope α was found to be -0.70 (little different than what is obtained from 492 regions, $\alpha = -0.71$). This result is in agreement with previous results by PSK88 and Kennicutt et al. (1989).

3.6. *Lyman Continuum Emission Rate and Star Formation Rate*

The observed Hα + [N II] luminosities of the H II regions in M81 with S/N $\geq$ 3 σ range from 3.9×10^{36} to 1.2×10^{39} ergs s^{-1}. Applying an average extinction of $A_V = 1.1 \pm 0.4$ mag (cf. Kaufman et al. 1987) for the H II regions, we find a correction factor to the Hα + [N II] luminosities should be $10^{0.320A_V} \simeq 2.2$ (Rieke & Lebofsky 1985). Assuming Brocklehurst (1970) case B recombination and neglecting absorption by He, the required Lyman continuum emission rate, Q_{Lyc}, is estimated to be

$$Q_{\mathrm{Lyc}} = (7.32 \times 10^{11}) L_{\mathrm{H}\alpha}\left(\frac{T_e}{10^4\ \mathrm{K}}\right)^{0.11}\ \mathrm{s}^{-1}$$

(Osterbrock 1989). For $T_e = 10^4$ K, we find Q_{Lyc} ranges from 2.6×10^{48} to 1.9×10^{51} s^{-1}.

Stellar synthesis models suggest that the star formation rate (SFR) is related to $L_{\mathrm{H}\alpha}$ by

$$\mathrm{SFR} = \frac{L_{\mathrm{H}\alpha}(\mathrm{total})}{1.12 \times 10^{41}\ \mathrm{ergs\ s^{-1}}}\ M_\odot\ \mathrm{yr}^{-1}$$

(Kennicutt 1983). Using this conversion factor, and taking the Hα + [N II] luminosity of M81 to be 3.5×10^{40} ergs s^{-1}, we obtain a SFR of $\sim$0.31 $M_\odot$ yr^{-1}. With extinction correction, this value becomes $\sim$0.68 $M_\odot$ yr^{-1}, or 3.6 times higher than the value of 0.19 $M_\odot$ yr^{-1} obtained by Hill et al. (1995) from space-based UV observations (applying to their data the same extinction value as we use).

4. SUMMARY

As part of the ongoing BATC survey, Hα + [N II] emission measurements of the H II regions of M81 in this paper are made to test our methodology of calibrating these fluxes. Our methods take advantage of both spectra and the well-calibrated intermediate-band images we have obtained of this galaxy in neighboring passbands. We also employ our previously well-tested background subtraction techniques (developed over the past few years by our team) to reduce uncertainties associated with continuum subtraction of the narrowband image centered on Hα + [N II]. We find the zero-point uncertainty of Hα + [N II] flux is close to 8% for bright H II regions. A comparison of our results with those PSK88 uncovers a systematic error in their fluxes as a function of position on their photographic plates. As a result, a new, more accurate catalog of the Hα + [N II] emission from the H II regions in M81 is given. The total Hα + [N II] emission luminosity for 456 H II regions is $\sim 8.7 \times 10^6$ $L_\odot$. The differential power-law function of number of the H II regions per logarithmic flux interval is investigated, and the slope of that power law is found to be -0.70, consistent with previous work. The derived SFR for all of the H II regions is $\sim$0.68 $M_\odot$ yr^{-1}, 3.6 times higher than that previously obtained from UV-based studies (Hill et al. 1995).

W. P. L. acknowledges supports from NKBRSF G1999075402 and the Shanghai NSF grant 02ZA4093. W. P. L. thanks the exchange program between Chinese Academic of Sciences and Max-Planck Society and the hospitality from Max-Planck-Institut für Astrophysik. The authors also thank the anonymous referee for helpful comments. This work is supported partly by the NSFC grants 19833020 and 10203004 and by the US NSF grant INT-9301805.

REFERENCES

Adler, D. S., & Westpfahl, D. J. 1996, AJ, 111, 735
Bertin, E., & Arnouts, S. 1996, A&AS, 117, 393
Brocklehurst, M. 1970, MNRAS, 148, 417
Davidge, T. J., & Courteau, S. 1999, AJ, 117, 2781
Devereux, N. A., Jacoby, G., & Ciardullo, R. 1995, AJ, 110, 1115
Fan, X., et al. 1996, AJ, 112, 628
Freedman, W. L., et al. 1994, ApJ, 427, 628
Garnett, D. R., & Shields, G. A. 1987, ApJ, 317, 82
Greenawalt, B., Walterbos, R. A. M., Thilker, D., & Hoopes, C. G. 1998, ApJ, 506, 135
Grossan, B., Gorjian, V., Werner, M., & Ressler, M. 2001, ApJ, 563, 687
Hill, J. K., et al. 1992, ApJ, 395, L37
———. 1995, ApJ, 438, 181
Hodge, P. W., & Kennicutt, R. C. 1983a, AJ, 88, 296
———. 1983b, ApJ, 267, 563
Immler, S., & Wang, Q. D. 2001, ApJ, 554, 202

Kaufman, M., Bash, F. N., Kennicutt, R. C., & Hodge, P. W. 1987, ApJ, 319, 61
Kaufman, M., Kennicutt, R. C., & Bash, F. N. 1986, IAU Symp. 116, Luminous Stars and Associations in Galaxies, ed. C. H. de Loore, A. J. Willis, & P. Laskarides (Dordrecht: Reidel), 503
Keel, W. C. 1989, AJ, 98, 195
Kennicutt, R. C. 1983, ApJ, 272, 54
Kennicutt, R. C., Jr., Edgar, B. K., & Hodge, P. W. 1989, ApJ, 337, 761
Kong, X., Lin, W. P., Zhou, X., Chen, F. Z., & Chen, J. S. 1999, Prog. Nat. Sci., 9, 1083
Kong, X., et al. 2000, AJ, 119, 2745
Lasker, B. M., Sturch, C. R., McLean, B. J., Russell, J. L., Jenkner, H., & Shara, M. M. 1990, AJ, 99, 2019
Oke, J. B., & Gunn, J. E. 1983, ApJ, 266, 713
Osterbrock, D. E. 1989, Astrophysics of Gaseous Nebulae and Active Galactic Nuclei (Mill Valley: Univ. Sci.)
Petit, H., Sivan, J.-P., & Karachentsev, I. D. 1988, A&AS, 74, 475 (PSK88)
Rieke, G. H., & Lebofsky, M. J. 1985, ApJ, 288, 618
Scoville, N. Z., Polletta, M., Ewald, S., Stolovy, S. R., Thompson, R., & Rieke, M. 2001, AJ, 122, 3017
Stauffer, J. R., & Bothun, G. D. 1984, AJ, 89, 1702
Wu, H., et al. 2002, AJ, 123, 1364
Yan, H. J., et al. 2000, PASP, 112, 691
Zheng, Z. Y., et al. 1999, AJ, 117, 2757
Zhou X., et al. 2003, A&A, 397, 361
Zhou, X., Jiang, Z.-J., Xue, S.-J., Wu, H., Ma, J., & Chen, J.-S. 2001, Chinese Astron. Astrophys., 1, 372